Journal of Solid State Chemistry 182 (2009) 3177–3182

Contents lists available at ScienceDirect

Journal of Solid State Chemistry

journal homepage: www.elsevier.com/locate/jssc

Porous cobalt oxide (Co_3O_4) nanorods: Facile syntheses, optical property and application in lithium-ion batteries

Rui Xu, Jiawei Wang, Qiuyu Li, Guoying Sun, Enbo Wang *, Siheng Li, Jianmin Gu, Mingliang Ju

Key Laboratory of Polyoxometalate Science of Ministry of Education, Department of Chemistry, Northeast Normal University, Ren Min Street No. 5268, Changchun, Jilin 130024, PR China

ARTICLE INFO

Article history:
Received 2 June 2009
Received in revised form
27 August 2009
Accepted 31 August 2009
Available online 11 September 2009

Keywords:
Co_3O_4 nanorods
Microemulsion
Scanning electron microscopy
Optical property
Lithium-ion batteries

ABSTRACT

We developed a facile synthetic route of porous cobalt oxide (Co_3O_4) nanorods via a microemulsion-based method in combination with subsequent calcination process. The porous structure was formed by controlled decomposition of the microemulsion-synthesized precursor CoC_2O_4 nanorods without destruction of the original morphology. The as-prepared Co_3O_4 nanorods, consisting of small nanoparticles with diameter of 80–150 nm, had an average diameter of 200 nm and a length of 3–5 μm. The morphology and structure of synthesized samples were characterized by transmission electron microscopy and scanning electron microscopy. The phase and composition were investigated by X-ray powder diffraction and X-ray photoelectron spectroscopy. The optical property of Co_3O_4 nanorods was investigated. Moreover, the porous Co_3O_4 nanorods exhibited high electrochemical performance when applied as cathode materials for lithium-ion batteries, which gives them good potential applications.

1. Introduction

As one of the most intriguing magnetic p-type semiconductors, Co_3O_4 of spinel structure is also known as a promising material that has applications in many fields, such as heterogeneous catalysts, solid-state sensors and electrochemical devices [1–6]. So far, a good many interesting nanostructures of Co_3O_4, including nanowires/nanorods [7,8], nanotubes [9,10], nanocubes [11–13], nanospheres [14–16], nanoplates [17] and nanowalls [18], have been achieved by different methods. Specially, porous Co_3O_4 materials have been reported as one of the cathode materials for lithium-ion batteries.

Since Poizot et al and Arico et al [19,20] reported on nanosized transition metal oxides as negtive electrode materials for lithium-ion batteries, considerable research has been focused on Co_3O_4 nanostructures in the past decade due to their high electrochemical performance. In particular, one dimension (1D) nanostructured materials have attracted a great deal of interest in the investigation of cathode materials for lithium-ion batteries due to their high surface area and short path length for Li^+ transport. For example, Liu et al reported the large-scale synthesis of Co_3O_4 nanowires by hydrothermal method and Li et al fabricated mesoporous Co_3O_4 nanowire (NW) arrays and applied them to lithium-ion batteries with the discharge capacity of about 1440 and 1150 mA h g^{-1}. [21,22]. More recently, Du et al synthesized the porous Co_3O_4 nanotube derived from $Co_4(CO)_{12}$ clusters on carbon nanotubes templates, which showed higher performance as lithium-ion battery electrodes with the discharge capacity of about 1918 mA h g^{-1} [23]. Therefore, it is reasonable to believe that 1D porous Co_3O_4 materials with higher surfaces may exhibit more potential applications in high-performance lithium-ion battery electrodes than amorphous bulk Co_3O_4.

In this study, we report a simple approach for the synthesis of Co_3O_4 nanorods via a microemulsion-based method in combination with calcination at 450 °C for 3 h. The porous structure was formed by controlled decomposition of the microemulsion-synthesized precursor CoC_2O_4 nanorods. The mechanism for the formation of Co_3O_4 nanorods was discussed. Additionally, the as-prepared Co_3O_4 nanorods have been used as cathode materials for lithium-ion batteries, which exhibit good cycle life and a high total discharge capacity of about 1171 mA h g^{-1}, which is much higher than the theoretical capacity of bulk Co_3O_4.

2. Experimental section

2.1. Materials

Cetyltrimethylammonium bromide (CTAB), cyclohexane, n-pentanol, $CoCl_2 \cdot 6H_2O$ and $H_2C_2O_4$ purchased from Beijing

* Corresponding author. Fax: +86 431 85098787.
E-mail addresses: wangeb889@nenu.edu.cn, wangenbo@public.cc.jl.cn (E. Wang).

0022-4596/$ - see front matter © 2009 Elsevier Inc. All rights reserved.
doi:10.1016/j.jssc.2009.08.033

Chemicals Co. Ltd. were of analytical grade and used as received without further purification.

2.2. Synthesis

There are various methods to synthesize porous cobalt oxides [24–28]. In this paper, a quaternary microemulsion, CTAB/water/cyclohexane/n-pentanol, was selected for this study. As a typical synthesis, the microemulsion was prepared by dissolving CTAB (2 g) in 50 mL of cyclohexane and 2.0 mL of n-pentanol. The resulting solution was stirred for 30 min until it became transparent. Subsequently, 3.0 ml of 0.8 M $H_2C_2O_4$ aqueous solution was added into the above solution and the mixture was stirred for another 1 h. Then, 1.0 ml of 0.05 M $CoCl_2$ aqueous solution was added in a dropwise manner to the above microemulsion and stirred for 24 h. The pink solid CoC_2O_4 product was collected by centrifugation. Finally, the precursor CoC_2O_4 was dried in an oven at 80 °C overnight and then calcined at 450 °C for 3 h, leading to the formation of the final Co_3O_4 nanorods.

2.3. Characterizations

The powder X-ray diffraction (XRD) data of the as-prepared samples were collected on a Rigaku D/max-IIB X-ray diffractometer at a scanning rate of 4°/min with 2θ ranging from 10° to 90° (Cu$K\alpha$ radiation λ=1.5418 Å). The morphology and microstructure of the as-prepared samples were observed by transmission electron microscopy (TEM) and the selected area electron diffraction (SAED) using a Hitachi-7500 electron microscope at an accelerating voltage of 120 kV and by scanning electron microscopy (SEM) using JEOL JSM-840 electron microscopes at an accelerating voltage of 20 kV. High-resolution transmission electron microscopy (HRTEM) image of Co_3O_4 nanorods was taken on a JEOL-2010 transmission electron microscope. Nitrogen (N_2) adsorption–desorption isotherms were measured at liquid nitrogen temperature (77 K) using a Nova l000 analyzer. The sample was degassed for 6 h at 150 °C before the measurements. Surface areas were calculated by the Brunauer–Emmett–Teller (BET) method from the data in the (P/P_0) region 0.05–0.35 and pore sizes by the Barrett–Joyner–Halenda (BJH) method at a relative pressure of 0.95 (P/P_0). X-ray photoelectron spectroscopy (XPS) and energy-dispersive X-ray (EDX) analyses have been done in order to obtain information about the chemical composition of the as-prepared samples. Optical absorption spectrum was recorded with a 756 CRT UV–vis spectrophotometer.

2.4. Electrochemical properties of Co_3O_4 nanorods

The electrochemical performances of Co_3O_4 as a cathode material were evaluated using two-electrode cells with lithium metal as the counter and reference electrodes. The working electrode was composed of 80 wt% the active materials (Co_3O_4), 10 wt% the conductive material (acetylene black, ATB) and 10 wt% binder (polytetrafluoroethylene, PTFE). The coated electrodes were dried (in vacuum) at 80 °C for 1 h and cut into a disk with a surface area of 1.0 cm^{-2}. The electrolyte solution was 1 M $LiPF_6$ dissolved in a mixture of ethylene carbonate (EC), propylene carbonate (PC) and diethyl carbonate (DEC) at a volume ratio of EC/PC/DEC=3:1:1. The cyclic voltammogram (CV) were obtained at a scan rate of 1 mV s^{-1} in the range of 0.01–3.0 V. The electrode capacity was measured by a galvanostatic discharge–charge method at a current density of 50 mA g^{-1} and a temperature of 20 °C on an electrochemical test instrument (CT2001A, Wuhan Land Electronic Co. Ltd., China).

3. Results and discussion

3.1. Phase and morphology of the synthesized Co_3O_4 nanorods

Fig. 1 shows the XRD patterns of Co_3O_4 nanorods and their precursor. As shown in Fig. 1a, no obvious XRD diffraction peak is found in the precursor CoC_2O_4 nanorods, indicating that CoC_2O_4 nanorods are amorphous in nature. After calcination at 450 °C for 3 h, the product exhibits sharp diffraction peaks (Fig. 1b). All the diffraction peaks can be perfectly indexed to the crystalline cubic phase Co_3O_4 with a lattice constant of a=8.083 Å (JCPDS, no. 42-1467). No diffraction peaks of other impurities are detected.

Fig. 2 shows the TEM images of Co_3O_4 nanorods and their precursor CoC_2O_4. As observed in Fig. 2a and b, the precursor CoC_2O_4 is composed of rod-like nanostructures with smooth surfaces. The CoC_2O_4 nanorods are around 200 nm in diameter and several of micrometers in length. Fig. 2c and d display low-magnification and high-magnification TEM images of the

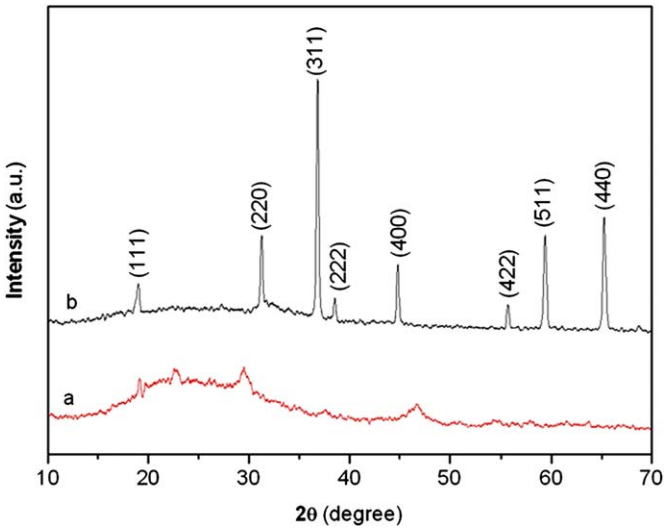

Fig. 1. The wide-angle XRD patterns of (a) the amorphous precursor composite of rod-like CoC_2O_4 nanostructures and (b) the synthesized spinel Co_3O_4 nanorods.

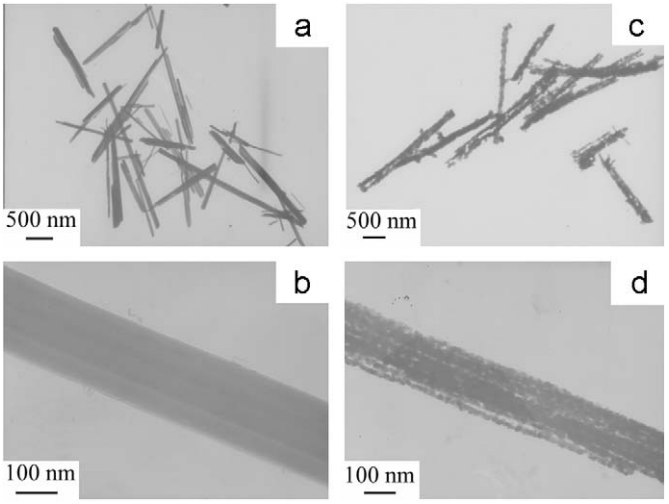

Fig. 2. Low-magnification (a) and high-magnification (c) TEM images of the amorphous precursor composite of rod-like CoC_2O_4 nanostructures. Low-magnification (b) and high-magnification (d) TEM images of the prepared Co_3O_4 nanorods.

as-prepared Co_3O_4 nanorods. During the whole calcination process, it could be seen that the product Co_3O_4 nanorods retained its original rod-like morphology of their precursor CoC_2O_4 In other words, this growth process can be regarded as a morphologically templated nucleation process [29–31]. The as-prepared Co_3O_4 nanorods with diameter of 150–250 nm and length of 3–5 μm are straight (Fig. 2c) with a porous structure (Fig. 2d). The porous structure is ascribed to the controlled decomposition of the microemulsion-synthesized precursor CoC_2O_4 nanorods. More details will be discussed below.

Fig. 3 shows low-magnification and high-magnification SEM images of the as-prepared Co_3O_4. Low-magnification SEM image (Fig. 3a) shows the overall morphology of Co_3O_4 nanorods. It could also be seen that the product retained its original rod-like morphology of the precursor CoC_2O_4 nanorods through the whole calcination process. The final Co_3O_4 sample is composed of uniform nanorods with a mean diameter of ~200 nm and an average length of 3–5 μm, which indicates that the aspect ratio is 25 or so. High-magnification SEM image (Fig. 3b) shows that the surfaces of Co_3O_4 nanorods are rough and these nanorods are stacked with smaller nanoparticles with diameter of 80–150 nm. Furthermore, irregular pores can be observed on the surfaces of these nanorods. It clearly confirms that the product consisted of uniform nanorods and the diameter and length of nanorods are in good agreement with those observed in TEM (Fig. 2c and d). Fig. 3c shows the EDX spectrum of the product. Co and O signals come from the as-prepared Co_3O_4 nanorods, and the percentages of Co and O are 56.83% and 43.17%, respectively. Furthermore, the ratio of Co and O is about 3:3.95 consistent with the theoretical value of Co_3O_4. The Pt signal comes from the coating material.

The high-magnification TEM image in Fig. 4a clearly indicates that Co_3O_4 nanorods consist of individual nanocrystals by bounding with each other. The SAED pattern (insert in Fig. 4a) shows that Co_3O_4 nanorods behave as a polycrystalline phase. Fig. 4b shows the HRTEM image of an individual Co_3O_4 nanorod. The lattice fringes with a lattice spacing of about 0.463 nm correspond to the {111} plane of cubic Co_3O_4, which are consistent with the the XRD results.

The gas adsorption–desorption method was also employed to confirm the porosity of Co_3O_4 nanorods. Fig. 5a depicts the N_2 adsorption–desorption isotherm of Co_3O_4 nanorods, indicating the existence of pores on the surface of Co_3O_4 nanorods. The BET surface area is as high as 115.27 m^2/g calculated from the data in

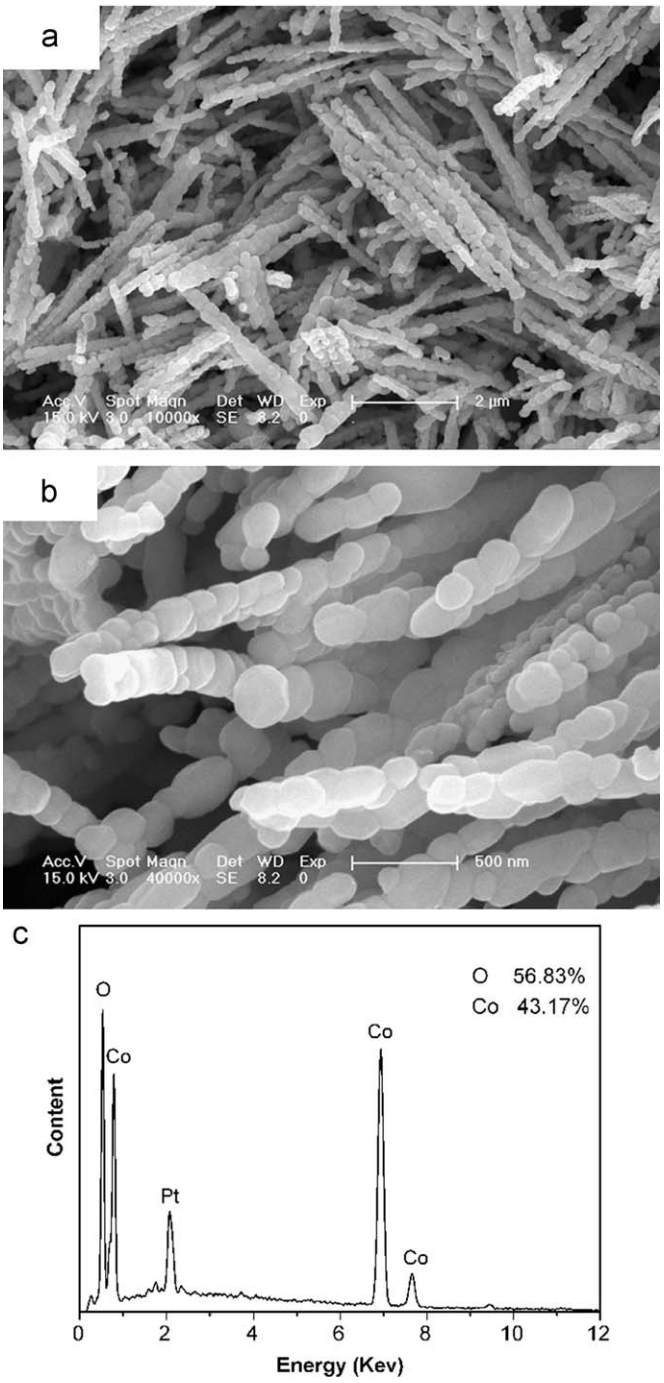

Fig. 3. Morphological and structural characterization of the spinel Co_3O_4 nanorods: (a) and (b) SEM images and (c) EDX spectrum.

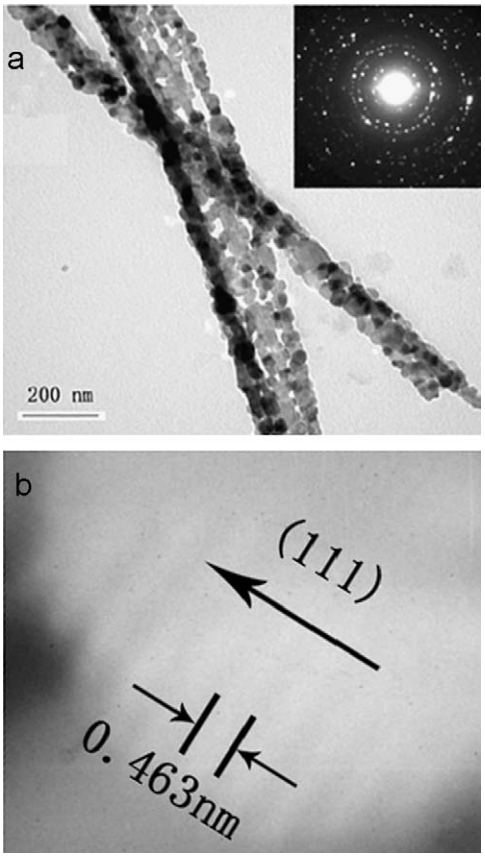

Fig. 4. (a) The high-magnification TEM image and SAED pattern (the insert) and (b) the HRTEM image of as-prepared Co_3O_4 nanorods.

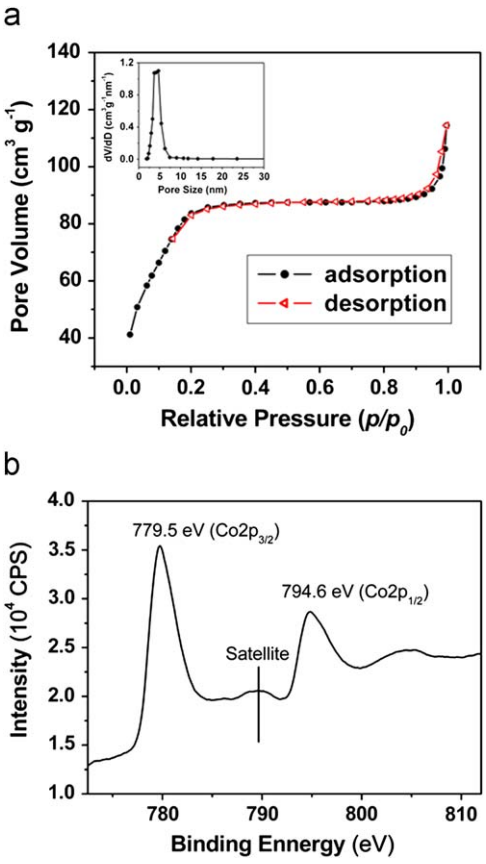

Fig. 5. (a) Nitrogen adsorption–desorption isotherms and pore-size distribution curve (the insert) and (b) the XPS pattern of the as-prepared spinel Co_3O_4 nanorods.

the (P/P_0) region of 0.05–0.35. The insert in Fig. 5a shows the BJH pore-size distribution curve of Co_3O_4 nanorods, exhibiting pore size focusing in the range of 3.6–5 nm. These mesopores should originate from the interstices among the small spheric nanoparticles [32], in agreement with the SEM observations of Co_3O_4 nanorods (Fig. 3a and b).

To further confirm the conclusion, the XPS of Co_3O_4 nanorods has also been measured. The Co 2*p* XPS spectrum (Fig. 5b) shows two major peaks with binding energy (BE) values at 794.6 and 779.5 eV, corresponding to the Co $2p_{1/2}$ and Co $2p_{3/2}$ spin–orbit peaks of the Co_3O_4 phase, respectively [33]. A satellite peak at 789.4 eV, about 9.9 eV higher than the position of the main peak of Co $2p_{3/2}$, is clearly detected in the spectrum. It is a typical satellite peak of the Co_3O_4 phase [34]. Thus, the results of XPS are consistent with those observed in the XRD and the EDX.

3.2. Growth mechanism of the nanostructured Co_3O_4 nanorods

As a polar surfactant, CTAB dissolve with their polar groups at the hydrocarbon–water interface of the micelle. Hence, they decrease the surface charge density of ionic micelles and thereby promote the formation of micellar geometries with lower mean curvature like rods [35]. The microemulsion-based method has recently been widely used to fabricate a large amount of 1D nanostructures with well-controlled morphology and size [36,37]. In our experiment, a similar method is used to prepare Co_3O_4 nanorods in combination with subsequent calcination. The procedure for the synthesis of Co_3O_4 nanorods is illustrated in Scheme 1. The formation of Co_3O_4 nanorods may result from the

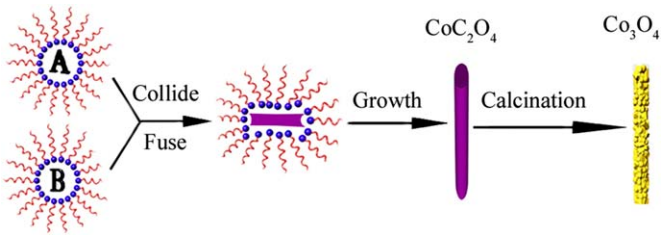

Scheme 1. The schematic diagram for the growth process of Co_3O_4 nanorods.

transformation of a lamellar precursor directed by the surfactant templates [30]. The microemulsion system is a critical selection for the directional growth and alignment of Co_3O_4 nanorods.

The possible formation mechanism can be understood as following, similar to the preparation of BaF_2 nanofibers and NiO [38,39]. After mixing the two microemulsion solutions containing $CoCl_2$ and $H_2C_2O_4$, the precursor CoC_2O_4 nuclei were formed by the precipitation of Co^{2+} cations with $C_2O_4^{2-}$ anions. During the nucleation process, the surfactant molecules on surfaces of the cylindrical droplet are adsorbed onto the surface planes of the formed CoC_2O_4 nuclei, resulting in the 1D growth of the homogeneous precursor composites of rod-like CoC_2O_4 nanostructure. As a consequence, the dryness and subsequent calcination lead to the formation of porous Co_3O_4 nanorods. In our experiment, only ionic surfactants (CTAB) are utilized to generate the microemulsion. Hence, CTAB is indispensable for the growth of Co_3O_4 nanorods, which plays dual roles. On the one hand, CTAB serves as an emulsifier for the generation of 1D amorphous precursor composites. On the other hand, CTAB serves as a low-temperature organic molten-salt medium for the directional alignment during the early stage of calcination. The two-step reaction process can be described as follows:

$$Co^{2+}\,(aq)+C_2O_4^{2-}\,(aq)\rightarrow CoC_2O_4\,(s) \quad (1)$$

$$3CoC_2O_4\,(s)+2O_2\,(g)\rightarrow Co_3O_4\,(s)+6CO_2\,(g) \quad (2)$$

Figs. 2 and 3 indicate that Co_3O_4 nanorods are transformed from the amorphous precursor nanorods without destruction of the original morphology through the whole calcination progress. The growth of crystalline Co_3O_4 nanorods is largely guided along the axial direction of the amorphous precursor CoC_2O_4 nanorods. To some extent, this growth process can be viewed as a morphologically templated nucleation process [30]. However, the nanostructural change is initiated by the coalescence of crystalline nanoparticles generated by the continuous decomposition of CoC_2O_4 at a relatively high temperature within the rods. During aggregation progress, the crystalline lattice planes may perfectly aligned or dislocated at the contact areas between the adjacent particles that generate the defects (Fig. 4a) in the finally formed crystal [31]. It is clear that the "oriented attachment" could play a role in the growth of crystalline nanorods during calcination. Therefore, the formation of nanorods is also possible through a directional coalescence process.

3.3. Optical absorption of Co_3O_4 nanorods

Fig. 6a shows the optical absorption spectrum of Co_3O_4 nanorods. Absorptions I (λ=760 nm) and II ($\lambda<500$ nm) are associated with ligand–metal charge transfer of O(−II)→Co(II) and O(−II)→Co(III), respectively [40]. The absorption band gap Eg can be obtained by the following equation:

$$(\alpha h\nu)^2 = B(h\nu - \mathrm{Eg}) \quad (3)$$

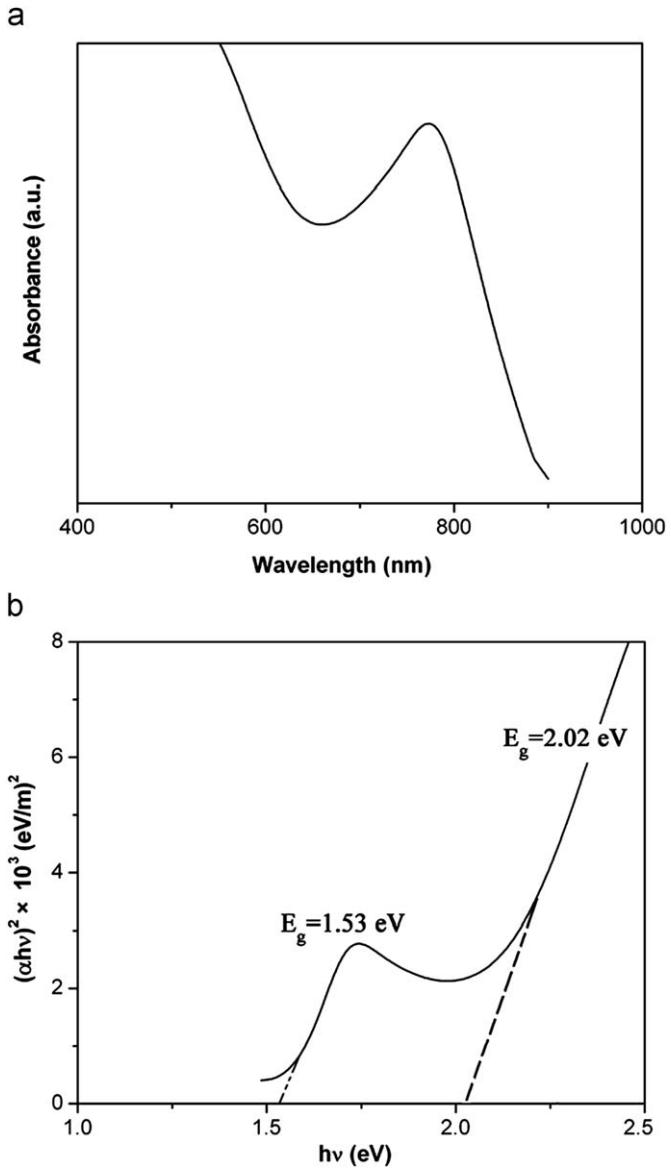

Fig. 6. (a) Optical absorption spectrum and (b) $(\alpha h\nu)^2 \sim h\nu$ curve for the as-synthesized Co_3O_4 nanorods.

where α is the absorption coefficient, $h\nu$ is the photo energy, B is a constant relative to the material, and the exponent n can take different values depending on the types of electronic transitions in the k-space. Fig. 6b gives the $(\alpha h\nu)^2$ versus $h\nu$ curve. As can be seen, the two optical band gaps of Co_3O_4 nanorods are 1.53 (Eg_1) and 2.02 eV (Eg_2), which are in good agreement with the Co_3O_4 band structure [41]. This suggests that the as-prepared Co_3O_4 nanorods are semiconducting with direct transitions at these energies. Eg_1 is associated with the onset of $O(-II) \rightarrow Co(III)$ excitations. Eg_2 is attributed to interband transition and regarded as the "true" energy gap.

3.4. Electrochemical properties of Co_3O_4 nanorods

Poizot et al [19] has proposed that the electrochemical reaction mechanism of lithium with transition metal oxides such as Co_3O_4 is a displacive redox reaction, which is different from the classic mechanism [42]. The electrochemical reaction mechanism of Li with Co_3O_4 nanorods in lithium-ion batteries can be described as follows:

$$Co_3O_4 + 8Li^+ + 8e^- \leftrightarrow 4Li_2O + 3Co^0 \quad (4)$$

$$8Li \leftrightarrow 8Li^+ + 8e^- \quad (5)$$

$$Co_3O_4 + 8Li \infty \overset{\text{discharge}}{\underset{\text{charge}}{\rightleftharpoons}} 4Li_2O + 3Co^0 \quad (6)$$

It is indicated that the electrochemical reaction of Li with Co_3O_4 nanorods is involved in the formation and decomposition of Li_2O, accompanying the reduction and oxidation of mental nanoparticles.

Fig. 7a shows the first three cyclic voltammogram (CV) curves of the electrodes made from Co_3O_4 nanorods with a scan rate of 1 mV s^{-1} at 20 °C. As could be seen, during the cathodic polarization process, there are two reduction peaks that can be attributed to two complete multistep redox reactions. During the following anodic polarization process, only one peak is recorded at about 2.2 V corresponding to an oxidation of Co^0 to Co^{3+}. Moreover, the intensity and position of peaks remain almost constant in all the CV cycles, indicating excellent cycle stability of Co_3O_4 nanorods electrode.

Fig. 7b shows the 1st and 10th discharge curves of the electrodes made from Co_3O_4 nanorods at a current density of 50 mA g^{-1} and a temperature of 20 °C. In both the 1st and 10th discharge curves, it could be seen that the potential rapidly dropped and reached a plateau of about 1.1 V, and then continuously decreased to 0 V. This is similar to the previous

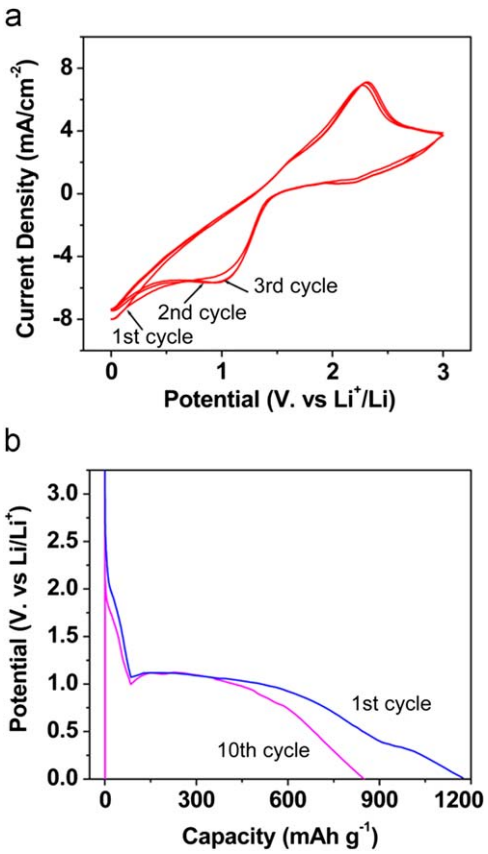

Fig. 7. Electrochemical properties of the prepared spinel Co_3O_4 nanorods. (a) First three CV curves of the Co_3O_4 nanorod-based negative electrode materials at a scan rate of 1 mV s^{-1} and a temperature of 20 °C, (b) the first and 10th discharge curves of the Co_3O_4 nanorod-based negative electrode materials at a current density of 50 mA g^{-1} and a temperature of 20 °C.

report [43]. In the first discharge curve, the initial capacity is 1171 mA h g^{-1}, which is much larger than the theoretical capacity of bulk Co_3O_4 [44]. From the first cycle, the discharge capacity gradually decreased in the following cycles. After 10 cycles, the discharge capacity maintained at about 850 mA h g^{-1}, which exhibited good cyclic life of the porous Co_3O_4 nanorods electrode and it was in good agreement with the CV results. It is reasonable to conclude that the porous Co_3O_4 nanorods, which comprised of smaller nanoparticles with size of about 80–150 nm, are responsible for the high electrochemical performance.

The superior electrochemical performance of Co_3O_4 nanorods electrode may be ascribed to the unique nanostructure of the as-prepared Co_3O_4 nanorods and smaller particles constructing the Co_3O_4 nanorods. The 1D nanostructure of Co_3O_4 nanorods can accommodate and lighten the stress caused by volume change and suppress the degradation of the electrode during the cycling process [45]. Moreover, the 1D nanostructure of Co_3O_4 nanorods can also hinder the aggregation of electrode materials, resulting in participation in the electrochemical reaction of every particle constituting the Co_3O_4 nanorods. All these possibly contribute to the large lithium storage capacity.

4. Conclusions

In summary, porous Co_3O_4 nanorods with 200 nm in diameter and several micrometers in length have been fabricated via a microemulsion-based method in combination with calcination at 450 °C for 3 h. Controlled decomposition of the microemulsion-synthesized precursor CoC_2O_4 nanorods is critical for the formation of the porous structure. The as-prepared Co_3O_4 nanorods exhibit higher capacity and better cycle life in lithium-ion battery than bulk Co_3O_4.

Acknowledgement

This work was financially supported by the National Natural Science Foundation of China (nos. 20701005/20701006), the Science and Technology Development Project Foundation of Jilin Province (no. 20060420), the Postdoctoral station Foundation of Ministry of Education (no. 20060200002), the Testing Foundation of Northeast Normal University and the Program for Changjiang Scholars and Innovative Research Team in University.

References

[1] Y. Yu, C.H. Chen, J.L. Shui, S. Xie, Angew. Chem. Int. Ed. 44 (2005) 7085–7089.
[2] Y.G. Li, B. Tan, Y.Y. Wu, J. Am. Chem. Soc. 128 (2006) 14258–14259.
[3] T. Maruyama, S. Arai, J. Electrochem. Soc. 143 (1996) 1383–1386.
[4] L. Yan, X.M. Zhang, T. Ren, H.P. Zhang, X.L. Wang, J.S. Suo, Chem. Commun. (2002) 860–861.
[5] E.M. Logothesis, R. Park, A.H. Meitzler, K.K. Laud, Appl. Phys. Lett. 26 (1975) 209–211.
[6] J. Wollenstein, M. Burgmair, G. Plescher, T. Sulima, J. Hildenbrand, H. Bottner, I. Eisele, Sensors Actuators B 93 (2003) 442–448.
[7] B.Z. Tian, X.Y. Liu, H.F. Yang, S.H. Xie, C.Z. Yu, B. Tu, D.Y. Zhao, Adv. Mater. 15 (2003) 1370–1374.
[8] Y.K. Liu, G.H. Wang, C.K. Xu, W.Z. Wang, Chem. Commun. (2002) 1486–1487.
[9] T. Li, S.G. Yang, L.S. Huang, B.X. Gu, Y.W. Du, Nanotechnology (2004) 1479–1482.
[10] L.H. Hu, Q. Peng, Y.D. Li, J. Am. Chem. Soc. 130 (2008) 16136–16137.
[11] R. Xu, H.C. Zeng, J. Phys. Chem. B 107 (2003) 926–930.
[12] J. Feng, H.C. Zeng, Chem. Mater. 15 (2003) 2829–2835.
[13] T. He, D.R. Chen, X.L. Jiao, Y.L. Wang, Adv. Mater. 18 (2006) 1078–1082.
[14] A.M. Cao, J.S. Hu, H.P. Liang, W.G. Song, L.J. Wan, X.L. He, X.G. Gao, S.H. Xia J. Phys. Chem. B 110 (2006) 15858–15863.
[15] T. Ozkaya, A. Baykal, Y. Koseoglu, H. Kavas, Cent. Eur. J. Chem. 7 (2009) 410–411.
[16] F.F. Tao, C.L. Gao, Z.H. Wen, Q. Wang, J.H. Li, Z. Xu, J. Solid State Chem. 182 (2009) 1055–1060.
[17] Y.L. Hou, H.S. Kondoh, M.S. Shimojo, T. Kogure, T. Ohta, J. Phys. Chem. B 109 (2005) 19094–19098.
[18] T. Yu, Y.W. Zhu, X.J. Xu, Z.X. Shen, P. Chen, C.T. Lim, J.T.L. Thong, C.H. Sow, Adv. Mater. 17 (2005) 1595–1599.
[19] P. Poizot, S. Laruelle, S. Grugeon, L. Dupont, J.M. Tarascon, Nature 407 (2000) 496–499.
[20] A.S. Arico, P. Bruce, B. Scrosati, J.M. Tarascon, W.V. Schalkwijk, Nat. Mater. 4 (2005) 366–377.
[21] X.H. Liu, G.Z. Qiu, X.G. Li, Nanotechnology 16 (2005) 3035–3040.
[22] Y.G. Li, B. Tan, Y.Y. Wu, Nano Lett. 8 (2008) 265–270.
[23] N. Du, H. Zhang, B.D. Chen, J.B. Wu, X.Y. Ma, Z.H. Liu, Y.Q. Zhang, D.R. Yang, X.H. Huang, J.P. Tu, Adv. Mater. 19 (2007) 4505–4509.
[24] [a] C. Dickinson, W.Z. Zhou, R.P. Hodgkins, Y.F. Shi, D.Y. Zhao, H.Y. He, Chem. Mater. 18 (2006) 3088–3095;
[b] Y.Y. Shi, Y. Wan, R.Y. Zhang, D.Y. Zhao, Adv. Funct. Mater. (2008) 2436–2443.
[25] [a] H. Tüysüz, Y. Liu, C. Weidenthaler, F. Schüth, J. Am. Chem. Soc. 130 (2008) 14108–14110;
[b] H. Tüysüz, M. Comotti, F. Schüth, Chem. Commun. (2008) 4022–4024.
[26] [a] J.H. Smått, B. Spliethoff, J.B. Rosenholm, M. Lindén, Chem. Commun. (2004) 2188–2189;
[b] G. Binotto, D. Larcher, A.S. Prakash, R.H. Urbina, M.S. Hegde, J.-M. Tarascon, Chem. Mater. 19 (2007) 3032–3040.
[27] [a] W.B. Yue, W.Z. Zhou, J. Mater. Chem. 17 (2007) 4947–4952;
[b] B.Y. Geng, F.M. Zhan, C.H. Fang, N. Yu, J. Mater. Chem. (2008) 4977–4984.
[28] G.X. Wang, X.P. Shen, J. Horvat, B. Wang, H. Liu, D. Wexler, J. Yao, J. Phys. Chem. C 113 (2009) 4357–4361.
[29] H.L. Zhu, X.Y. Gu, D.T. Zuo, Z.K. Wang, N.Y. Wang, K.H. Yao, Nanotechnology, 19 (2008) 405503.
[30] Z.T. Zhang, A.J. Rondinone, J.X. Ma, J. Shen, S. Dai, Adv. Mater. (2005) 1415–1419.
[31] C. Pacholski, A. Kornowski, H. Weller, Angew. Chem. Int. Ed. (2002) 1188–1191.
[32] Q.F. Zhang, T.P. Chou, B. Russo, S.A. Jenekhe, G.Z. Cao, Angew. Chem. Int. Ed. 47 (2008) 2402–2406.
[33] M. Oku, Y. Sato, Appl. Surf. Sci. 55 (1992) 37–41.
[34] Z. Dong, Y.Y. Fu, Q. Han, Y.Y. Xu, H. Zhang, J. Phys. Chem. C (2007) 18475–18478.
[35] M. Tornblom, U. Henrikesson, J. Phys. Chem. B 101 (1997) 6028–6035.
[36] J.H. He, T.H. Wu, C.L. Hsin, K.M. Li, L.J. Chen, Y.L. Chueh, L.J. Chou, Z.L. Wang, Small 2 (2006) 116–120.
[37] J. Zhou, Y. Ding, S.Z. Deng, L. Gong, N.S. Xu, Z.L. Wang, Adv. Mater. 17 (2005) 2107–2110.
[38] M.H. Cao, C.W. Hu, E.B. Wang, J. Am. Chem. Soc. 125 (2003) 11196–11197.
[39] W.G. Tian, P.P. Wang, L. Ren, G.B. Sun, L.N. Sun, K. Yang, B.Q. Wei, C.W. Hu J. Solid State Chem. 180 (2007) 3551–3559.
[40] D. Barreca, C. Massign, S. Daolio, M. Fabrizio, C. Piccirillo, L. Armelao E. Tondello, Chem. Mater. 13 (2001) 588–593.
[41] [a] P.S. Patil, L.D. Kadam, C.D. Lokhande, Thin Solid Films 272 (1996) 29–32;
[b] X. Wang, X.Y. Chen, L.S. Gao, H.G. Zheng, Z.D. Zhang, Y.T. Qian, J. Phys. Chem. B 108 (2004) 16401–16404.
[42] M. Yoshio, H.Y. Wang, K. Fukuda, Angew. Chem. Int. Ed. 42 (2003) 4203–4206.
[43] H. Zhang, J.B. Wu, C.X. Zhai, X.Y. Ma, N. Du, J.P. Tu, D.R. Yang, Nanotechnology 19 (2008) 035711.
[44] G.X. Wang, Y. Chen, K. Konstantinov, M. Lindsay, H.K. Liu, S.X. Dou, J. Power Sources 109 (2002) 142–147.
[45] W.Y. Li, F.Y. Cheng, Z.L. Tao, J. Chen, J. Phys. Chem. B 110 (2006) 119–124.